Prediction of the Molecular Mechanism of Corni Fructus-Epimedii Folium-Rehmanniae Radix Praeparata in the Treatment of Postmenopausal Osteoporosis Based on Network Pharmacology and Molecular Docking

Yu Zhou[1,2,3,#], Xin Li[3,#], Jinchao Wang[4], Rong He[3], Liqi Ng[2], Dapeng Li[4], Jeremy Mortimer[2,5], Swastina Nath Varma[2], Jinhua Hu[3], Qing Zhao[6], Zeyu Peng[3], Chaozong Liu[2,*] and Songchuan Su[1,*]

[1]Chongqing Orthopedic Hospital of Traditional Chinese Medicine, Chongqing, 400012, China; [2]Institute of Orthopaedic and Musculoskeletal Science, University College London, Royal National Orthopaedic Hospital, Stanmore, London HA7 4LP, UK; [3]Changchun University of Chinese Medicine, Changchun, 130117, China; [4]Yantai Hospital of Shandong Wendeng Osteopathic & Traumatology, Yantai, 264009, China; [5]School of Anatomy, University of Bristol, Southwell Street, Bristol, BS2 8EJ, UK; [6]Tianjin University of Chinese Medicine, Tianjin, 301617, China

Abstract: ***Introduction*:** In this study, core drugs of clinical postmenopausal osteoporosis were retrieved using data mining, the drug molecular action target was predicted through network pharmacology, the key nodes of interaction were identified by combining postmenopausal osteoporosis-related targets, and the pharmacological mechanism of Traditional Chinese Medicine (TCM) against postmenopausal osteoporosis and other action mechanisms was explored.

***Methods*:** TCMISS V2.5 was used to collect TCM prescriptions of postmenopausal osteoporosis from databases, including Zhiwang, Wanfang, PubMed, *etc*., for selecting the highest confidence drugs. TCMSP and SwissTargetPrediction databases were selected to screen the main active ingredients of the highest confidence drugs and their targets. Relevant targets for postmenopausal osteoporosis were retrieved from GeneCards and GEO databases, PPI network diagrams construction and selection of core nodes in the network, GO and KEGG enrichment analysis, and molecular docking validation.

***Results*:** Correlation analysis identified core drug pairs as 'Corni Fructus-Epimedii Folium-Rehmanniae Radix Praeparata' (SZY-YYH-SDH). After TCMSP co-screening and de-weighting, 36 major active ingredients and 305 potential targets were selected. PPI network graph was built from the 153 disease targets and 24 TCM disease intersection targets obtained. GO, KEGG enrichment results showed that the intersectional targets were enriched in the PI3K-Akt signalling pathway, *etc*. The target organs were mainly distributed in the thyroid, liver, CD33+_Myeloid, *etc*. Molecular docking results showed that the core active ingredients of the 'SZY-YYH-SDH' were able to bind to the pair core nodes and PTEN and EGFR.

***Conclusion*:** The results showed that 'SZY-YYH-SDH' can provide the basis for clinical application and treat postmenopausal osteoporosis through multi-component, multi-pathway, and multi-target effects.

Keywords: Corni fructus, epimedii folium, rehmanniae radix praeparata, data mining, network pharmacology, postmenopausal osteoporosis.

*Address correspondence to these authors at the Chongqing Orthopedic Hospital of Traditional Chinese Medicine, Chongqing 400012, China and Institute of Orthopaedic and Musculoskeletal Science, University College London, Royal National Orthopaedic Hospital, Stanmore, London HA7 4LP, UK; E-mails: chaozong.liu@ucl.ac.uk and su_songchuan@sohu.com

[#]*These authors contributed equally to this work.*

1. INTRODUCTION

Postmenopausal osteoporosis (PMO) is a common systemic metabolic bone disease caused by a decline in ovarian function and insufficient oestrogen production after menopause, resulting in greater bone resorption than bone formation. Recent studies have shown that the pathogenesis of PMO is not exact. However, it is closely related to ageing, leading to lower estrogen levels [1], oxidative stress [2], intestinal flora [3], and iron overload [4, 5]. The clinical manifestations of PMO are mainly dominated by bone pain and susceptibility to fracture. Current treatments are mostly in the form of a nutritious and balanced diet, exercise, and various medications taken orally, *etc*. [6].

Data mining is a data analysis technique that can discover valid information from large amounts of data [7, 8]. Network pharmacology is a technique based on systems biology, multiple pharmacology, histology, and other disciplines to analyse biological systems and drug targets and select specific signalling nodes for multi-target drug molecule design [9]. Molecular docking is a technique for finding low-energy binding modes of ligands to known receptors through the characteristics of the receptor and the interactions between the receptor and the drug molecule [10].

Therefore, this study collects TCM commonly used in the clinical treatment of PMO through data mining techniques, analyses their drug composition, screens the core drugs, elucidates the mechanism of action and association between the drugs and the disease through network pharmacology and molecular docking methods, and analysis and predicts their possible mechanisms of action to provide some reference for subsequent treatment and research work in the clinical setting.

2. MATERIALS AND METHODS

2.1. Literature Data Mining

2.1.1. Documentary Sources

Searches were conducted in CNKI, VVIP, Pubmed, WanFang Database, and Web of Science databases for 'Postmenopausal Osteoporosis', 'PMO', 'Traditional Chinese Medicine', 'Chinese Medicine', and 'Integrative Chinese and Western Medicine', starting from the date of creation of each database to May 18th, 2022. All literature (6,135) was deweighted to obtain 3,454 documents, from which a total of 117 documents were screened for clinical observations that met the criteria, involving data extraction and entry by two independent personnel. The search and analysis processes are shown in Fig. (**1**).

2.1.2. Inclusion Criteria

(1) The sample must be clinical patients and must meet the diagnostic criteria for PMO in both Chinese and Western medicine; (2) The drugs used are oral compound preparations of TCM; (3) The trial design and statistical methods are scientifically valid; (4) Only one article with different names of the same formula or duplicate literature is included; (5) The name and dosage of the TCM must be clear in the literature; (6) The treatment efficiency must be ≥ 80%.

2.1.3. Exclusion Criteria

(1) Doctoral or master's theses, reviews, medical cases, test cases, case studies and other types of information, (2) animal experiments and basic research, (3) invalid test results or lack of clinical information, and (4) those with other diseases or complications.

2.1.4. Standardisation of TCM

The 2020 edition of the Chinese Pharmacopoeia is used as the standard to standardise the names of the TCM contained in the prescriptions, such as 'Glycyrrhizae Radix Et Rhizoma Praeparata Cum Melle' and 'Glycyrrhizae Radix Et Rhizoma' being standardised as 'Glycyrrhizae Radix Et Rhizoma', to prevent the analysis results from being affected by the different preparation methods or aliases of the drugs.

2.1.5. Prescription Entry and Data Analysis

The prescriptions that met the criteria were entered one by one into the module 'TCMISS V2.5 Software' - 'Platform Management' - 'Formulary Management' to create a 'PMO Formulary Database'. Two independent persons were responsible for entering the information and reviewing the data at the end of the entry. Traditional Chinese Medicine Inheritance Support System (TCMISS) V2.5 is widely used for the analysis of TCM prescription data. The software integrates general statistics, text mining, association rules, and entropy clustering methods for complex systems [11]. The frequency of drug use, flavour and meridian tropism, formula patterns, core combinations, and potential new prescriptions were analysed using the 'Data Analysis' and 'Statistical Reports' modules. The drug combination pattern with the highest confidence level was selected for the study of the mechanism of action.

2.2. Network Pharmacology and Molecular Docking Analysis

2.2.1. Screening of 'SZY-YYH-SDH' Active Compounds and Predicted Targets

The TCM Systems Pharmacology Database and Analysis Platform (https://tcmsp-e.com/) is a systems pharmacology platform for TCM, which provides interactive data on the relationships between drugs, targets, and diseases. The platform also provides information on the pharmacokinetic effects of chemicals, targets, and drug target networks as well as natural compounds, including drug similarity (DL), oral bioavailability (OB), intestinal epithelial permeability, water solubility, and blood-brain barrier permeability. OB ≥ 30% and DL values ≥ 0.18 were used as criteria for screening the active ingredients of SZY, YYH, and SDH TCM. Compounds meeting the OB and DL thresholds were used as active compounds for subsequent studies and analysis.

The 'Related targets' module in TCMSP was used to retrieve the relevant targets for the above active compounds and the UniProt (http://www.UniProt.org/) database was used to convert the target protein names to the official symbols of the gene targets. Active ingredients not present in the 'related targets' module were entered into the PubChem database, their Canonical SMILES sequence numbers were obtained and the SwissTargetPrediction database (http: //www.swisstargetprediction.ch) was used to predict their protein targets. The predicted targets were aggregated and

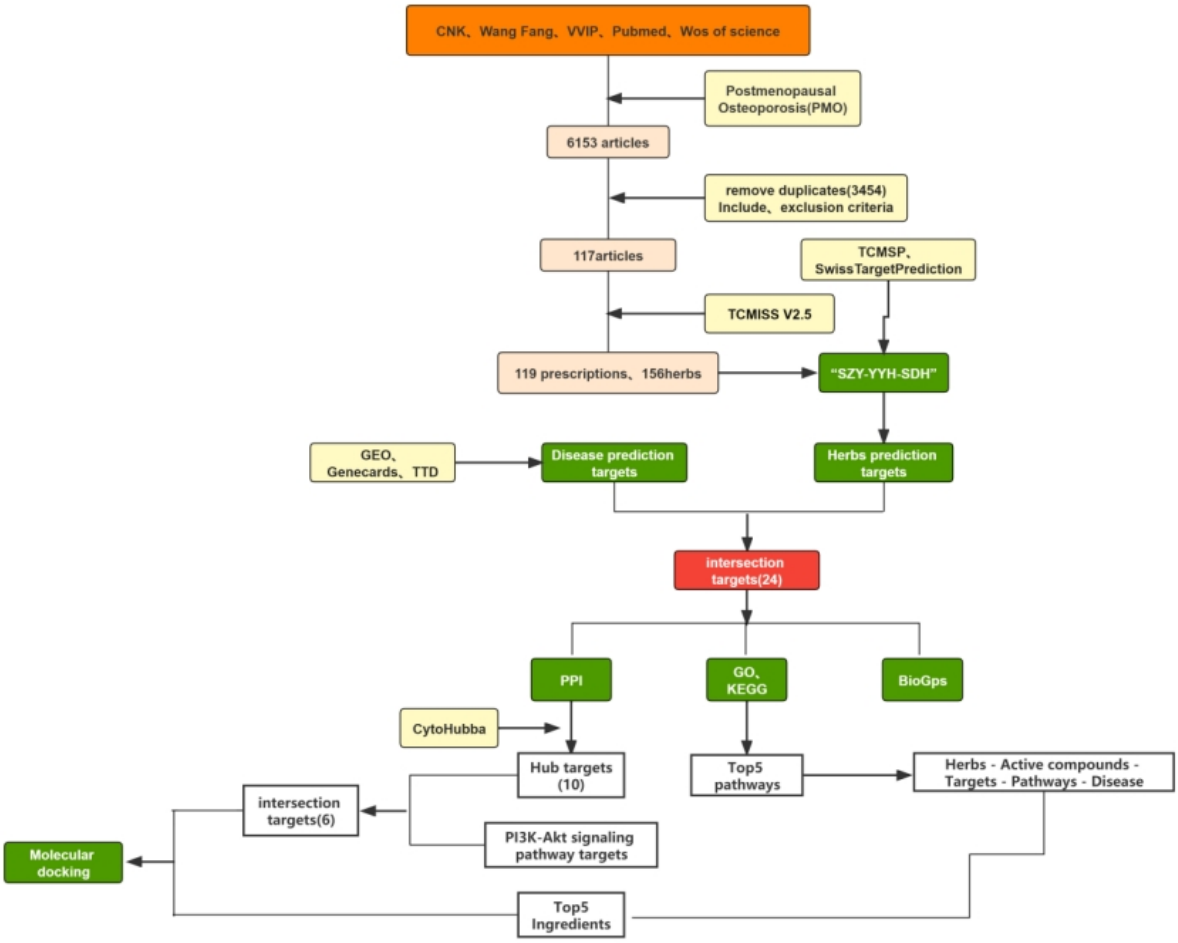

Fig. (1). Flowchart of retrieval analysis. *(A higher resolution / colour version of this figure is available in the electronic copy of the article).*

de-weighted to create the 'SZY-YYH-SDH' predicted target set by removing the components without targets. To scientifically and rationally explain the relationship between compounds and targets, Cytoscape 3.9.1 (https://www.cytoscape.org/) was used to construct the 'drugs-component-target' network interoperability map.

2.2.2. Establishment of a Database of PMO Disease Targets

Different series of samples were searched in the Gene Expression Omnibus dataset (GEO: www.ncbi.nlm.nih.gov/geo/) to obtain mRNA expression profiles between PMO and normal samples (GSE161361). Differential genes (DEGs) between disease and normal samples were detected using the platform's GEO2R with screening thresholds of $|logFC| > 1$ and $P < 0.05$, while volcano plots of DEGs were obtained. In addition, searches were performed in the GeneCards database (http://www.genecards.org/), and the Therapeutic Targets database (TTD, http://db.idrblab.net/ttd/) was used using the keyword Postmenopausal Osteoporosis and de-duplicated to create the PMO disease target dataset.

2.2.3. Construction and Parametric Analysis of Protein-protein Interaction (PPI) Networks

The intersection between the predicted targets of 'SZY-YYH-SDH' and PMO disease targets was obtained using the bioinformatics online tool (http: //www.bioinformatics.com.cn). The intersection targets were imported into the STRING database (http://string-db.org), with the species limited to 'Homo sapiens' and the confidence score set to ≥0.400. Then, it was saved in TSV format and imported into Cytoscape 3.9.1 software to construct a PPI network. Three key topological parameters were selected for the selection of core targets based on PPI networks: Degree centrality (DC), Closeness centrality (CC), and Betweenness centrality (BC). The values of the three parameters indicate the importance and influence of the relevant nodes in the whole network. The core nodes in the PPI network were selected according to the criteria of DC ≥ 2x median and CC and BC ≥ median.

2.2.4. GO, KEGG Enrichment Analysis and Target Organ network Analysis

The intersecting targets under '1.2.3' were entered into the DAVID database (https://david.ncifcrf.gov), which is useful for annotation, visualisation, and integrated discovery. Gene Ontology (GO) and Kyoto Encyclopedia of Genes and Genomes (KEGG) enrichment analyses were performed on the intersecting targets, and the GO and KEGG enrichment results were visualised using the online mapping platform Microsign. To elucidate the complex associations between TCM, active compounds, targets, pathways, and diseases, we

Table 1. TCM for PMO with a frequency ≥ 20.

Rank	Name of the Medicine	Frequency	Average Dose (g)	Rank	Name of the Medicine	Frequency	Average Dose (g)
1	Rehmanniae Radix Praeparata	78	22.67	13	Salviae Miltiorrhizae Radix Et Rhizoma	38	21.18
2	Epimedii Folium	75	14.00	14	Corni Fructus	37	11.94
3	Drynariae Rhizoma	61	13.95	15	Poria	36	17.38
4	Angelicae Sinensis Radix	57	14.92	16	Atractyodis Macrocephalae Rhizoma	31	12.32
5	Astragali Radix	56	21.82	17	Cuscutae Semen	28	18.46
6	Eucommiae Cortex	56	16.62	18	Chuanxiong Rhizoma	26	10.65
7	Achyranthis Bidentatae Radix	49	18.42	19	Paeoniae Radix Alba	25	14.52
8	Psoraleae Fructus	48	15.97	20	Codonopsis Radix	25	15.36
9	Dioscoreae Rhizoma	45	15.86	21	Cervi Cornus Colla	22	20.86
10	Lycii Fructus	43	16.86	22	Cistanches Herba	22	15.27
11	Glycyrrhizae Radix Et Rhizoma	43	7.23	23	Testudinis Carapax Et Plastrum	21	29.47
12	Dipsaci Radix	40	16.97	24	Morindae Officinalis Radix	21	11.90

Table 2. Statistics on the four qi and five flavours of drugs used in the treatment of PMO.

Rank	Four Qi	Frequency	Rank	Five Flavours	Frequency
1	Warm	807	1	Sweet	967
2	Neutral	372	2	Bitter	538
3	Cold	196	3	Pungent	471
4	Heat	36	4	Sour	129
5	Cool	33	5	Salty	83
-	-	-	6	Astringent	69

used Cytoscape 3.9.1 software to construct and analyse a 'drugs-active compound-target-pathway-disease' interaction network map.

2.2.5. Target Organ Network Construction

As the metabolism of 'SZY-YYH-SDH' *in vivo* is not known, its therapeutic effect on PMO may involve multiple organs, tissues, and immune cells in the body. Therefore, we used the BioGPS database (https://biogps.org) to analyse the mRNA levels of the intersecting targets under '1.2.3' in each organ and tissue. The data in BioGPS were obtained from microarray analysis. The target organ network was constructed using Cytoscape 3.9.1.

2.2.6. Molecular Docking Validation

The PDB format and SDF format of the receptor and ligand proteins were obtained from the RCSB PDB database (https://www.pdb.org/) and PubChem database (https://pubchem.ncbi.nlm.nih.gov/), respectively, and the format conversion was completed using OpenBabel 3.1.1 software. The molecular docking was verified by AutoDockTools 1.5.6 and Autodocak vina software, and dehydration and hydrogenation were performed using PyMOL software. The docking results were processed using PyMOL and Ligplot software, and the interaction and binding patterns were visualised [11-29].

3. RESULTS

3.1. Literature Mining Results

3.1.1. Frequency of Drugs

A total of 117 papers met the inclusion and exclusion criteria, from which 119 prescriptions involving a total of 156 drugs were extracted. The frequency of occurrence of each drug was counted, and a total of 24 drugs with a frequency ≥20 were listed, with the top 5 being Rehmanniae Radix Praeparata, Epimedii Folium, Drynariae Rhizoma, Angelicae Sinensis Radix and Astragali Radix, respectively (Table **1**).

3.1.2. Statistical Analysis of the Four qi, Five Tastes and Attribution of Drugs

Statistics on the four qi and five flavours of 156 drugs are presented in Table **2** and Figs. (**2A** and **B**). The frequencies of warm, neutral, cold, heat, and cool drugs were 807, 372, 196, 36, and 33, and the frequencies of sweet, bitter, pungent,

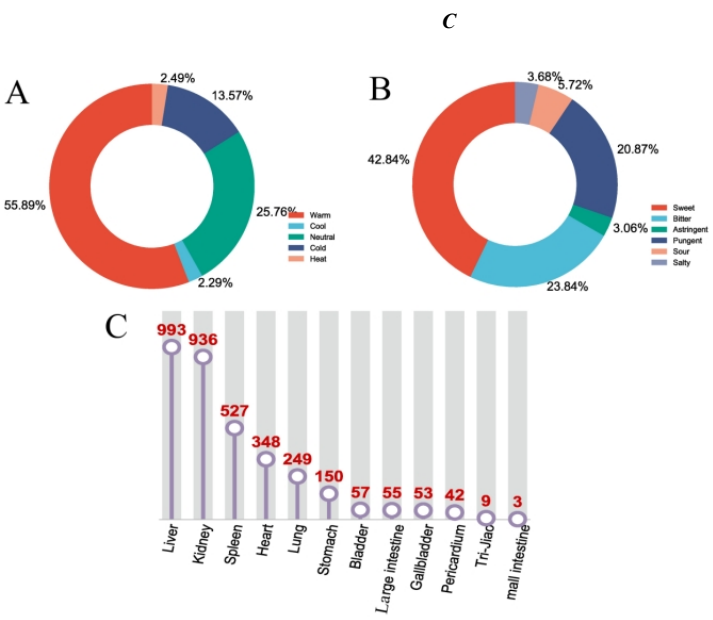

Fig. (2). Statistical diagrams of the four qi, five tastes, and the attribution of meridians in drugs for PMO. (**A**): Statistical chart of the Four Qi of Chinese herbal medicinal drugs for PMO; (**B**): Statistical chart of the five tastes of Chinese herbal medicinal drugs for PMO. (**C**): Statistical chart of the attribution of Chinese herbal medicinal drugs to the meridians for PMO. *(A higher resolution / colour version of this figure is available in the electronic copy of the article).*

Table 3. TCM for PMO with a frequency ≥20.

Rank	Core Portfolio 1	Rank	Core Portfolio 2	Rank	New Formulation Composition
1	Cibotii Rhizoma_Chaenomelis Fructus_Pinelliae Rhizoma	1	Cibotii Rhizoma_Chaenomelis Fructus_Radix Et Caulis Flemingiae	1	Cibotii Rhizoma_Chaenomelis Fructus_Pinelliae Rhizoma_Radix Et Caulis Flemingiae
2	Codonopsis Radix_Poria_Atractyodis Macrocephalae Rhizoma	2	Poria_Carthami Flos_Atractyodis Macrocephalae Rhizoma	2	Codonopsis Radix_Poria_Atractyodis Macrocephalae Rhizoma_Carthami Flos
3	Rehmanniae Radix Praeparata_Corni Fructus_Eupolyphaga Steleophaga	3	Dioscoreae Rhizoma_Corni Fructus_Alismatis Rhizoma_Moutan Cortex	3	Rehmanniae Radix Praeparata_Corni Fructus_Eupolyphaga Steleophaga_Dioscoreae Rhizoma_Alismatis Rhizoma_Moutan Cortex
4	Rehmanniae Radix Praeparata_Achyranthis Bidentatae Radix_Trionycis Carapax	4	Achyranthis Bidentatae Radix_Trionycis Carapax_Epimedii Folium	4	Rehmanniae Radix Praeparata_Achyranthis Bidentatae Radix_Trionycis Carapax_Epimedii Folium
5	Aconiti Lateralis Radix Praeparata_Cinnamomi Cortex_Asari Radix Et Rhizoma	5	Saposhnikoviae Radix_Cinnamomi Cortex_Cervi Cornu Degelatinatun	5	Aconiti Lateralis Radix Praeparata_Cinnamomi Cortex_Asari Radix Et Rhizoma_Saposhnikoviae Radix_Cervi Cornu Degelatinatun
6	Chuanxiong Rhizoma_Cuscutae Semen_Lycii Fructus	6	Chuanxiong Rhizoma_Cuscutae Semen_Cyperi Rhizoma	6	Chuanxiong Rhizoma_Cuscutae Semen_Lycii Fructus_Cyperi Rhizoma

sour, salty, and astringent drugs were 967, 538, 471, 129, 83, and 69, respectively. According to the statistics of the drug's meridians (Fig. **2C**), the top 5 meridians were liver, kidney, spleen, heart, and lung; among them, the frequency of the liver meridian was 993, the highest among them.

3.1.3. Analysis of Core Combinations and Composition of New Formulations

The data were analysed according to the number of prescriptions and drugs, combined with different correlation and penalty parameters. When the correlation degree was set to 8 and the penalty degree to 3, the results were more in line with clinical practice. Six groups each of 2 different core combinations were extracted by complex system entropy clustering analysis; based on the results of the improved mutual information method, the correlation coefficients between the two drugs were obtained by the analysis method of complex system entropy clustering, followed by cluster analysis to obtain 6 potential new prescriptions from 119 prescriptions (Table **3**).

3.1.4. Research on the Composition Pattern of Prescriptions based on Association Rule Analysis

Based on the Apriori association rule algorithm, the higher the number of support (the number of support is the frequency of drug combinations occurring in the selected

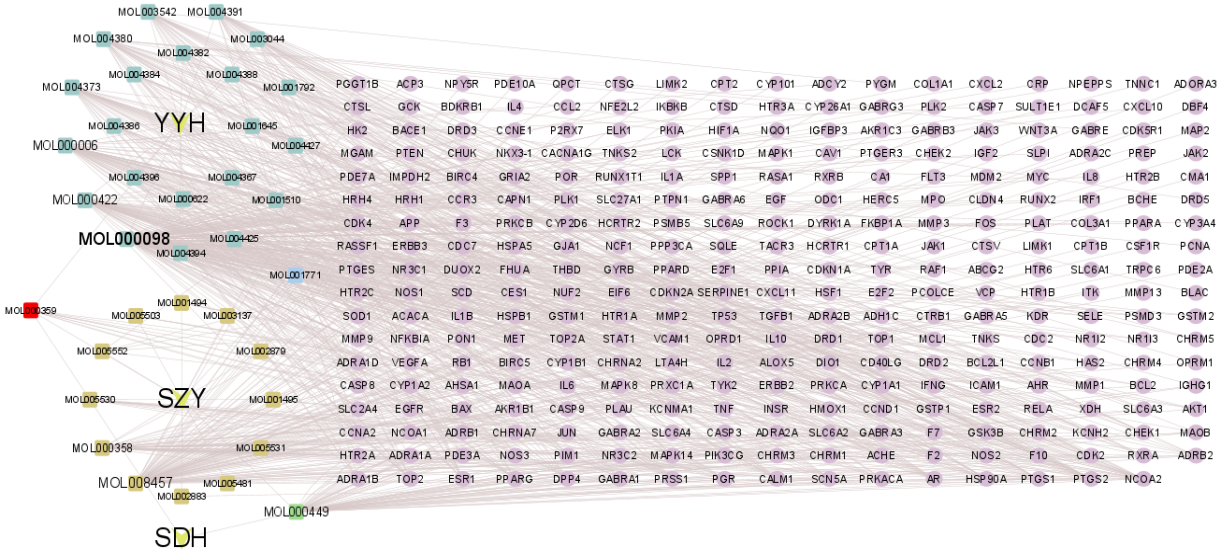

Fig. (3). Diagram of the drug-compound-target interaction network. *(A higher resolution / colour version of this figure is available in the electronic copy of the article).*

prescription), the better it reflects the association between the core drugs. The higher the confidence level (confidence level is the probability that the drug on the left side of the '→' appears at the same time as the drug on the right side) is close to 1, the more frequently the drug on the left side of the '→' appears at the same time as the drug on the right side. By using the system's 'pattern of combination' analysis function and setting the support level to 25 and the confidence level to 0.90, a total of 48 pairs of drug combination patterns with frequencies ≥ 25 were obtained, sorted in descending order of drug combination frequency (Table **S1**); at the same time, a total of three rules for the use of commonly used drugs were obtained (Table **4**).

Table 4. Statistics on core combinations and new formula composition in the treatment of PMO in TCM.

Rank	Medication Association Rules	Confidence
1	Corni Fructus→Rehmanniae Radix Praeparata	0.945945946
2	Corni Fructus, Epimedii Folium→Rehmanniae Radix Praeparata	0.961538462
3	Corni Fructus, Dioscoreae Rhizoma→Rehmanniae Radix Praeparata	0.931034483

As shown in Table **4**, 'SZY-YYH-SDH' was the highest confidence level, so this study focused on this dosing pattern to predict and analyse its specific mechanism of action.

3.2. Prediction and Analysis of the Mechanism of Action of Core Combinations

3.2.1. Active Compounds and Potential Targets of 'SZY-YYH-SDH'

A total of 45 active compounds of the three drugs 'SZY-YYH-SDH' were obtained from the TCMSP database, of which SZY, YYH, and SDH contained 20, 23, and 2 compounds, respectively, and 15, 23, and 2 compounds, respectively, after neglecting the components without predicted targets, for a total of 36 compounds after de-weighting. The TCMSP database and SwissTargetPrediction database were used to obtain the potential targets corresponding to the above active ingredients. Among them, 207 were SZY, 510 were YYH and 34 were SDH, for a total of 305 after de-duplication (Table **S2**). Each drug, its active compounds, and corresponding targets were imported into Cytoscape 3.9.1 to establish a 'drugs-compound-target' interactions network containing 344 nodes and 784 edges (Fig. **3**).

3.2.2. PMO Disease Targets

We screened for DEGs between PMO samples and normal samples in the GSE161361 dataset at |logFC| > 1 and P < 0.05 (Fig. **4A**). A total of 5580 genes (Table **S3**) were identified in the analysis, of which 3837 were up-regulated and 1743 were down-regulated. In addition, a total of 917 disease targets were obtained through the Genecards, TTD database, with 914 after de-duplication. A total of 153 cross-targets were obtained after intersecting the disease targets obtained from GEO with those from Genecards and TTD using the bioinformatics online tool (Fig. **4B**), which was used to build the PMO disease target dataset.

3.2.3. Construction and Analysis of PPI Networks

The intersection of PMO disease targets and the predicted targets of 'SZY-YYH-SDH' was obtained using the bioinformatics online tool, and a total of 24 cross-targets were obtained (Fig. **5A**). To explore the mechanism of action of 'SZY-YYH-SDH' in the treatment of PMO, the 24 targets were imported into the String database to construct a PPI network (Fig. **5B**). The network consisted of 110 nodes and 1108 edges with median DC, CC, and BC values of 6.500, 0.560, and 3.819, respectively. We selected 10 core targets based on topological analysis with the criteria of DC ≥ 2x median, CC and BC ≥ median (Table **S4**), from which the core target network was constructed (Fig. **5C**).

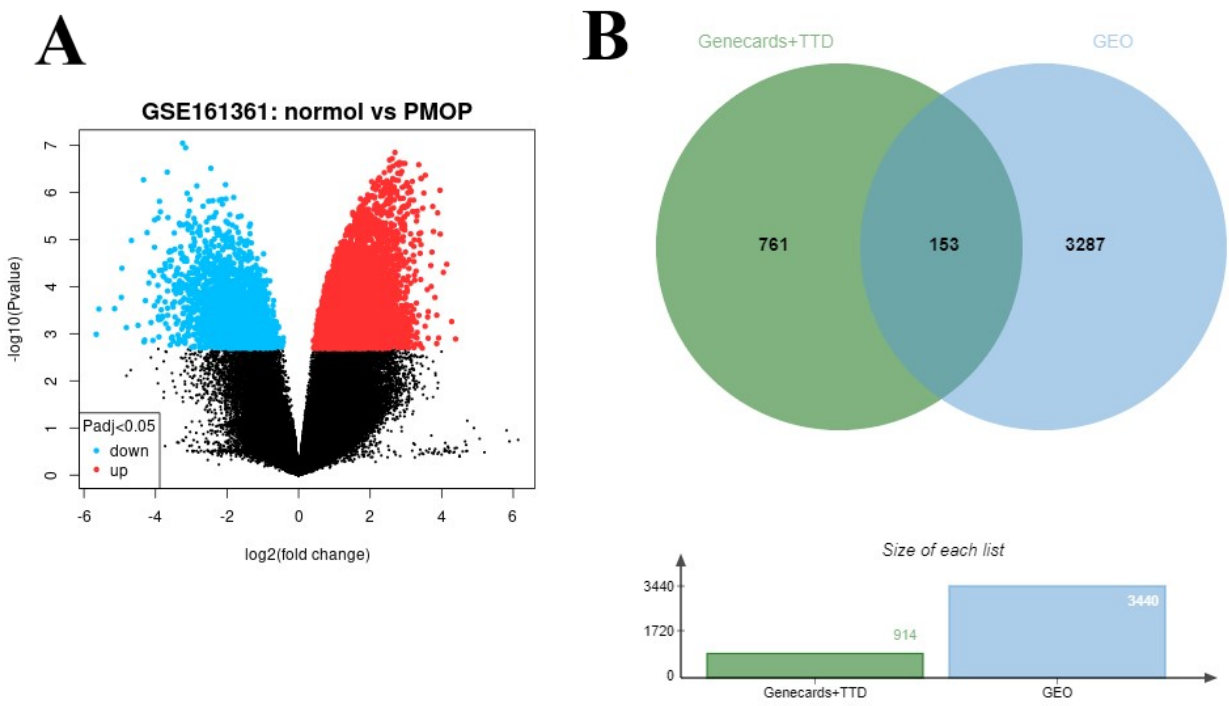

Fig. (4). DEG volcano map and disease target intersection map. (**A**): DEGs between PMOP samples and normal samples in the GSE161361 dataset; (**B**): Disease targets obtained by GEO were intersected with targets from Genecards and TTD to obtain a total of 153 cross-targets. *(A higher resolution / colour version of this figure is available in the electronic copy of the article).*

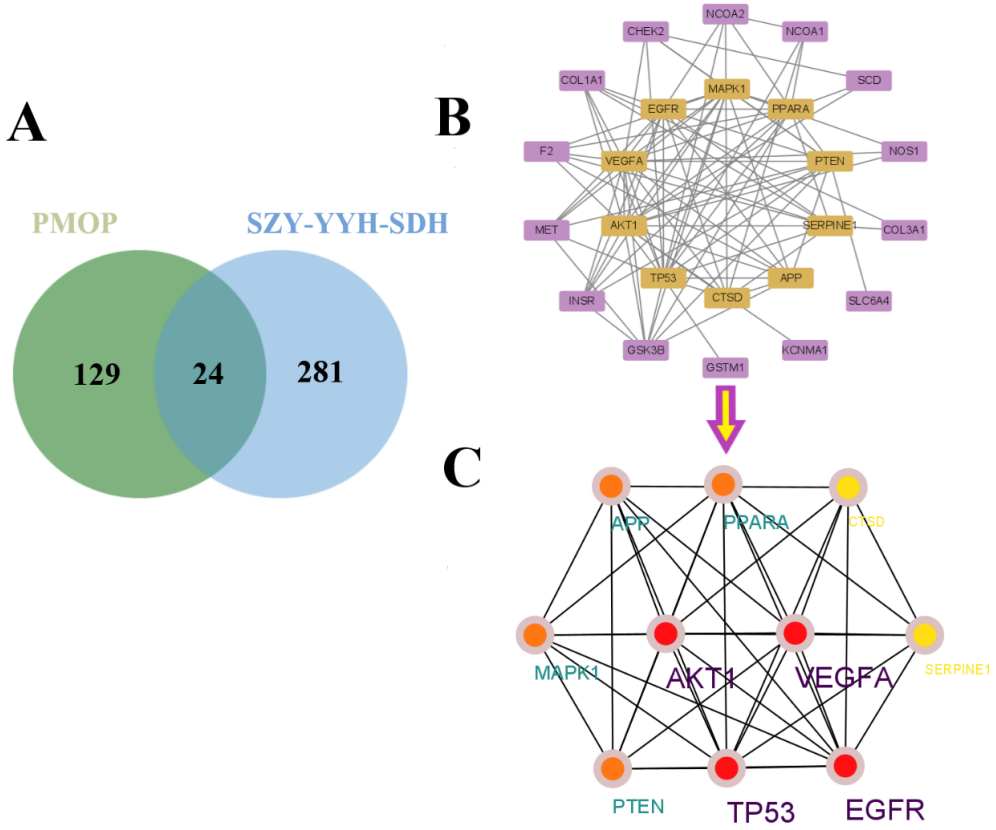

Fig. (5). Intersection target table, PPI network diagram, and core target network diagram. (**A**) PMO-'SZY-YYH-SDH' intersection target. (**B**) Intersection target PPI network diagram. (**C**) Core target network diagram. *(A higher resolution / colour version of this figure is available in the electronic copy of the article).*

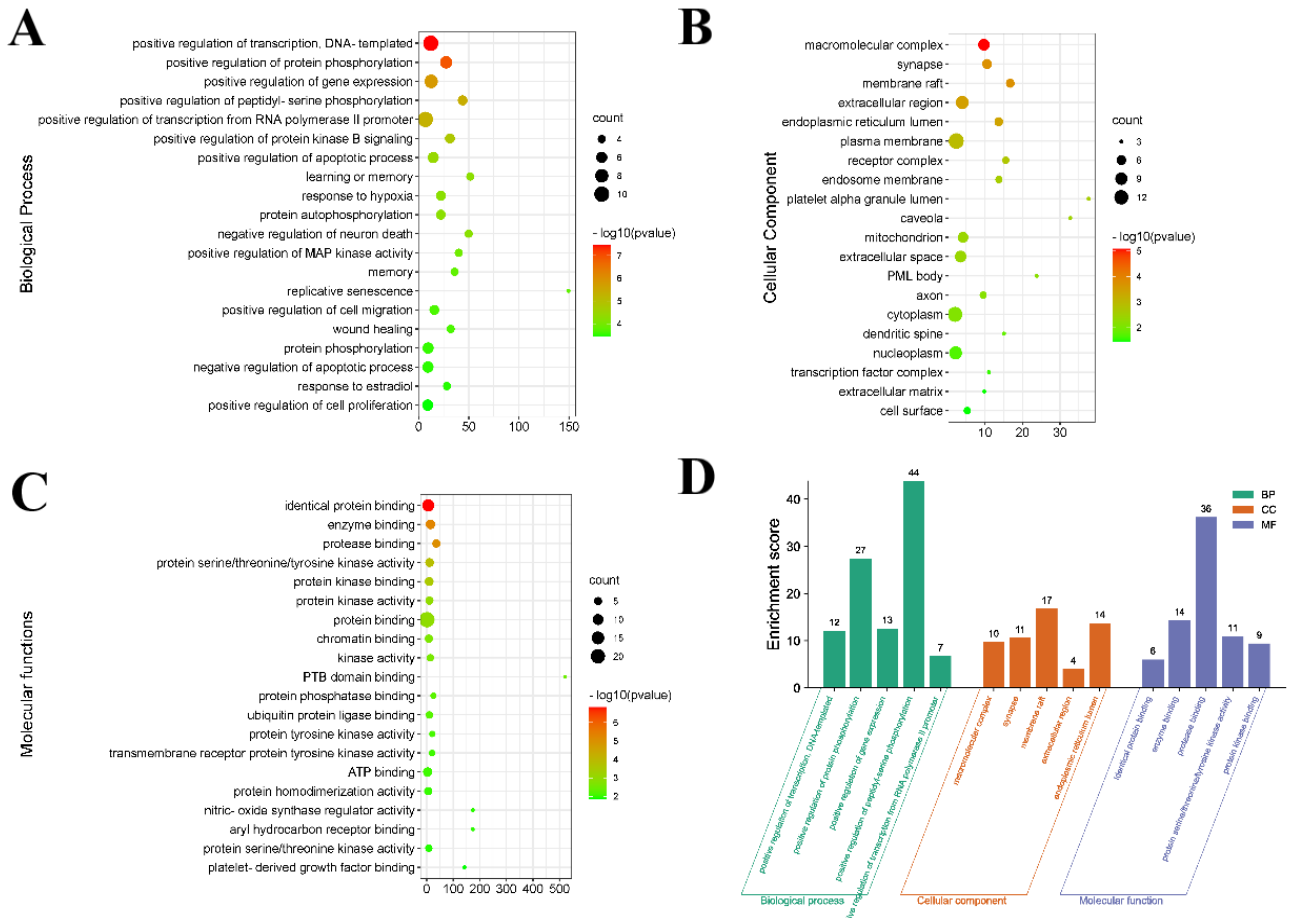

Fig. (6). Graphs of BP, MF, and CC enrichment results analysis. (**A**). BP with Top20 *P*-value values. (**B**). MF with Top20 *P*-value values. (**C**). CC with Top20 *P*-value values. (**D**). Histogram of Top 5 items with *P*-value values in BP, MF, and CC. *(A higher resolution / colour version of this figure is available in the electronic copy of the article).*

3.2.4. GO, KEGG Enrichment Analysis

We performed GO and KEGG enrichment analysis on 24 targets in the PPI network. The GO enrichment results included a total of three categories: biological process (BP), molecular function (MF), and cellular component (CC). Among them, 184 items were BP, 39 were MF, and 26 were CC. The top 20 BP, MF, and CC items in terms of *P*-value are shown in the form of bubble plots (Figs. **6A-C**). The top 5 *P*-Value ranked items in each category are presented in a bar chart (Fig. **6D**). The above information is summarized in Table (**S5**). BP mainly relates to the positive regulation of transcription, DNA-templated, positive regulation of protein phosphorylation, *etc*. MF relates to identical protein binding, enzyme binding, protease binding, *etc*. CC relates to macromolecular complex, synapse, membrane raft, *etc*.

Twenty-four common targets were assessed by KEGG pathway enrichment analysis (P <0.05 for significance level). They were enriched to a total of 83 pathways (Table **S6**). We visualized the pathways with the top 20 *P*-value values (Fig. **7A** and **B**). Among them, the pathway with the lowest *P*-value was EGFR tyrosine kinase inhibitor resistance, and the others were the PI3K-Akt signalling pathway, Hepatocellular carcinoma, Endometrial cancer, *etc*.

We selected five significant pathways from the KEGG enrichment analysis (PI3K-Akt signalling pathway, Focal adhesion, HIF-1 signalling pathway, Thyroid hormone signalling pathway, and Estrogen). The 'drugs-component-target-pathway-disease' network was mapped using Cytoscape 3.9.1 (Fig. **7C**). The network contained 48 nodes and 148 edges. The CytoHubba plug-in was used to analyse the parameters of each node in the network, and the top 5 targets, components, and pathways with Degree values are shown in the Table. The Sankey diagram was constructed using the bioinformatics online tool based on the linkage between target genes and enrichment pathways (Fig. **7D**), and the PI3K-Akt signalling pathway map was rendered using 'PathView' (Fig. **8**).

3.2.5. Target Organ Network Analysis

We assessed the mRNA levels of 24 targets in tissues and organs, which showed a significant increase in mRNA levels, mainly in 76 tissues and organs associated with PMO. Of these, those involving a high number of endocrine system targets were Thyroid (11), Pineal-night (12), Pineal-day (11), and PancreaticIslet (9); TestisSeminiferousTubule (9) in the male reproductive system, Prostate (11), Spinal cord (9) in the central nervous system, SmoothMuscle (10) in the vegetative

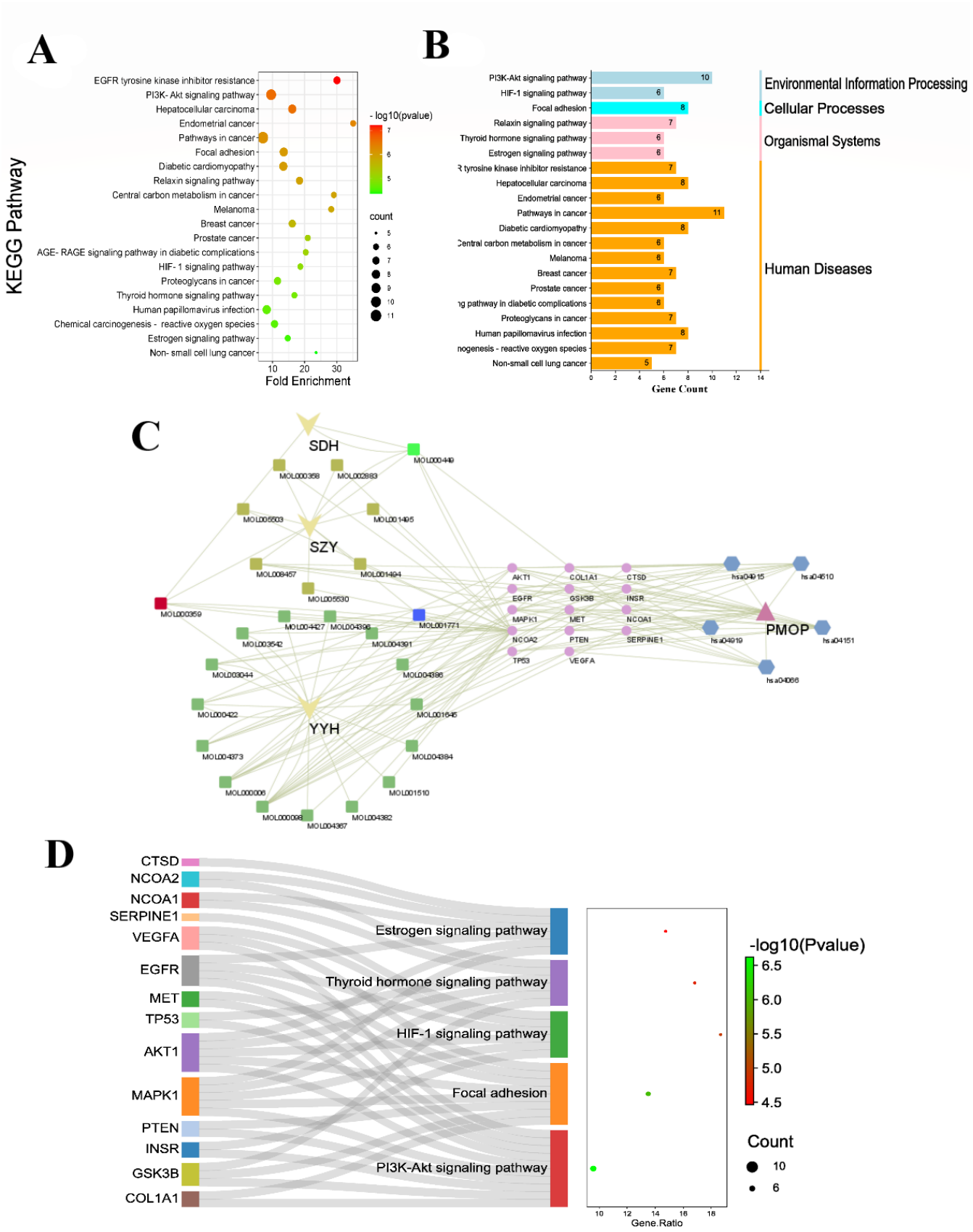

Fig. (7). 'Drugs - component - target - pathway - disease' network diagram pathway target analysis. (**A**, **B**). Pathways with top 20 *P*-value values. (**C**). Network diagram of' drugs - component - target - pathway - disease'. (**D**). Sankey diagram of top 5 pathways-targets with *P*-value. *(A higher resolution / colour version of this figure is available in the electronic copy of the article).*

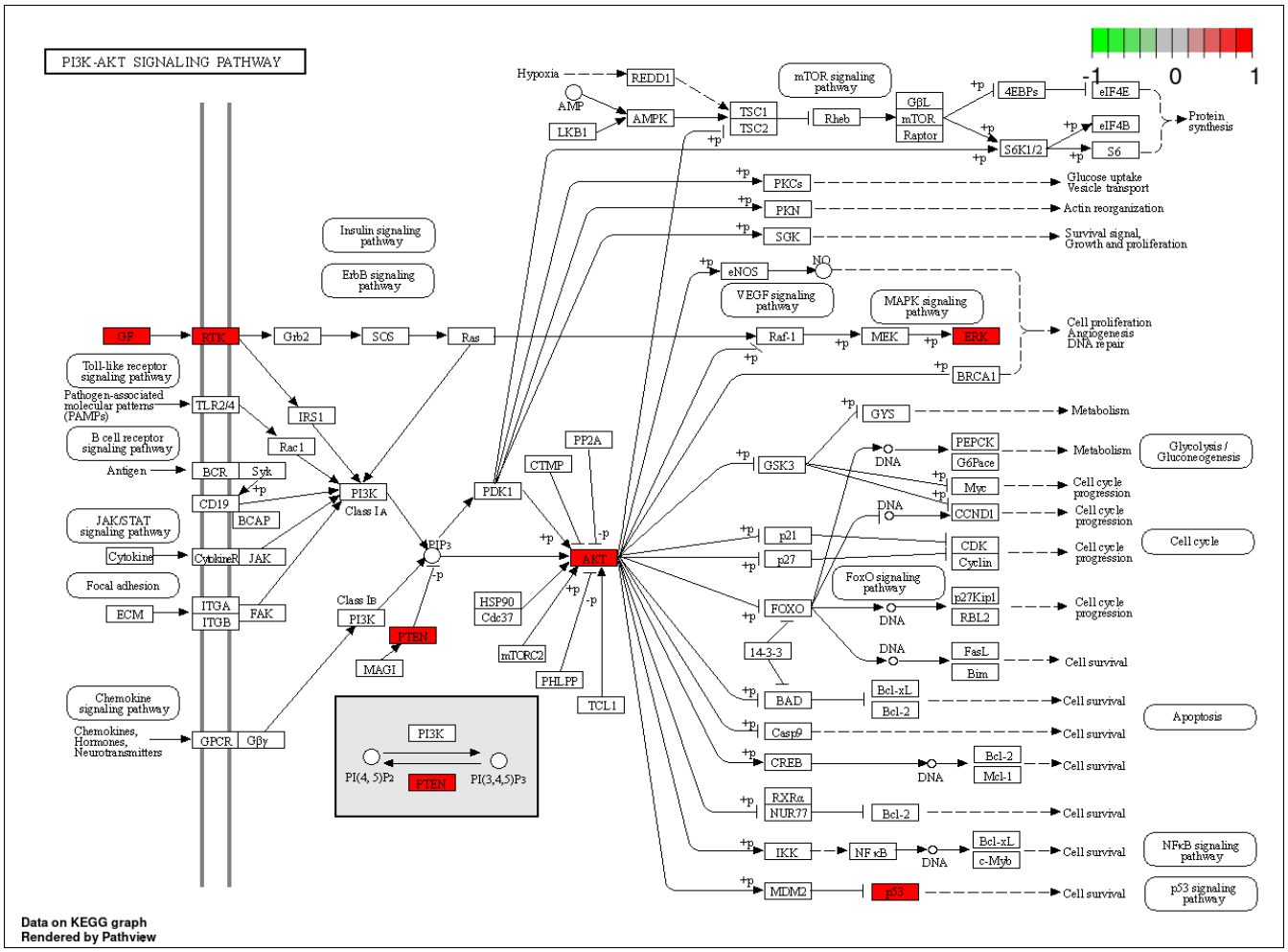

Fig. (8). PI3K-Akt signalling pathway rendering. *(A higher resolution / colour version of this figure is available in the electronic copy of the article).*

nervous system; 721_B_lymphoblasts (14), Lymphoma_burkitts (Raji) (9) in the lymphatic system (9); Lung (9) in the respiratory system; Liver (14), Colorectaladenocarcinoma (10), Colon (11) in the digestive system; Heart (10) in the circulatory system; CD105+_Endothelial (10), CD10 4_Monocytes (10), CD14+_Monocytes (10), CD33+_Mye loid (13), CD34+ (9), CD56+_NKCells (13) in the immune system. The results suggest that the therapeutic effect of 'SZY-YYH-SDH' on PMO may involve multiple systems in the body and that these tissues and organs are closely related to the targets of 'SZY-YYH-SDH' intervention. Target site and tissue organ information are provided in Table **S7**. The above information was used to construct the target-organ network diagram (Fig. **9**), which contains a total of 100 nodes and 455 edges.

3.2.6. Molecular Docking Validation

We evaluated the binding between the screened active drugs and targets by molecular docking to validate the above data mining and network pharmacology predictions. We crossed the targets enriched by the PI3K-Akt signalling pathway with the core nodes in the PPI network and selected six intersecting targets as the recipient pairs (VEGFA, TPP53, AKT1, EGFR, MAPK1, and PTEN). The top 5 active ingredients (Quercetin, Luteolin, Stigmasterol, Sitosterol, and Chryseriol) in the 'drugs-component-target-pathway-disease' network were used as docking ligands and their binding ability was predicted by AutoDock Tools software, as provided in Tables (**S8** and **S9**), respectively. The binding energy between each respective protein and compound was plotted as a heat map (Fig. **10**).

It is generally considered that binding energy <-1.2 kcal·mol-1 indicates good binding activity between receptors and ligands. In this study, receptors and ligands with binding energies ≤ -9.0 kcal·mol-1 were Quercetin-PTEN, Stigmasterol-EGFR, Stigmasterol- PTEN, Sitosterol - EGFR, Sitosterol - PTEN, and the docking results were visualized in 2D and 3D using Ligplot and Pymol software for their hydrogen bonding and hydrophobic interactions (Fig. **11**).

4. DISCUSSION

In this study, the literature on TCM for PMO was collected from multiple databases through the TCMISS V2.5 software. The prescriptions that met the criteria of 'oral' and 'Chinese medicinal preparation' were screened, and the drug combination with the highest confidence level, namely

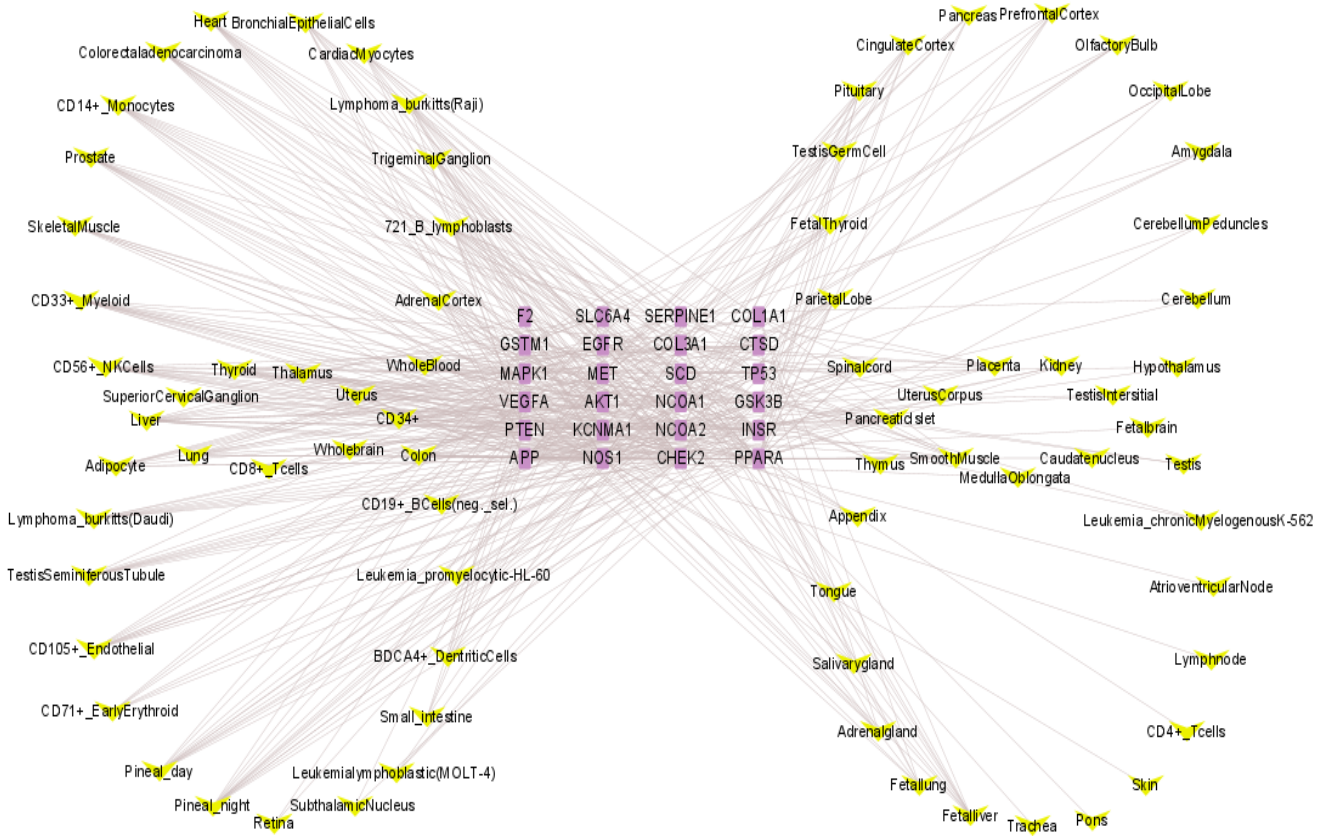

Fig. (9). 'SZY-YYH-SDH' - Target organ network distribution of PMO targets. *(A higher resolution / colour version of this figure is available in the electronic copy of the article).*

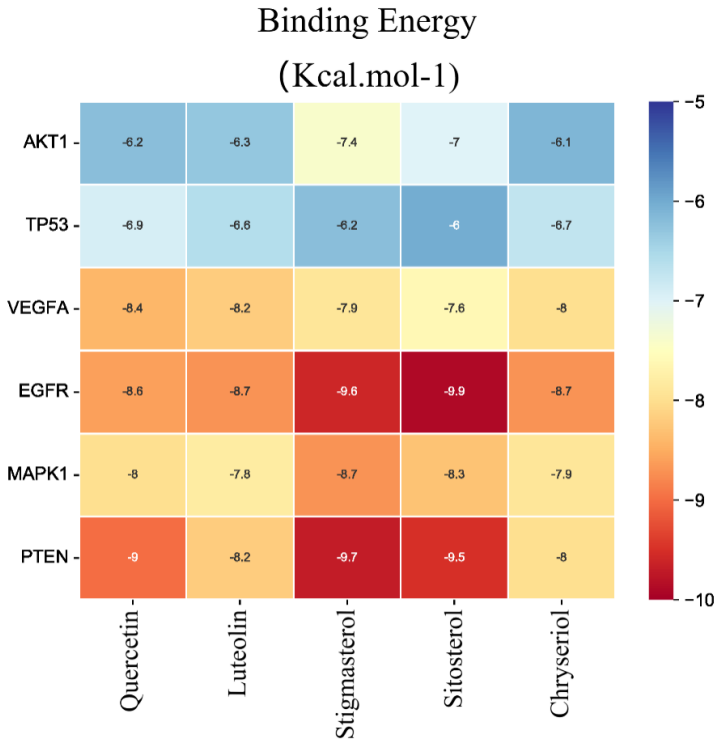

Fig. (10). Combined energy heat map analysis. *(A higher resolution / colour version of this figure is available in the electronic copy of the article).*

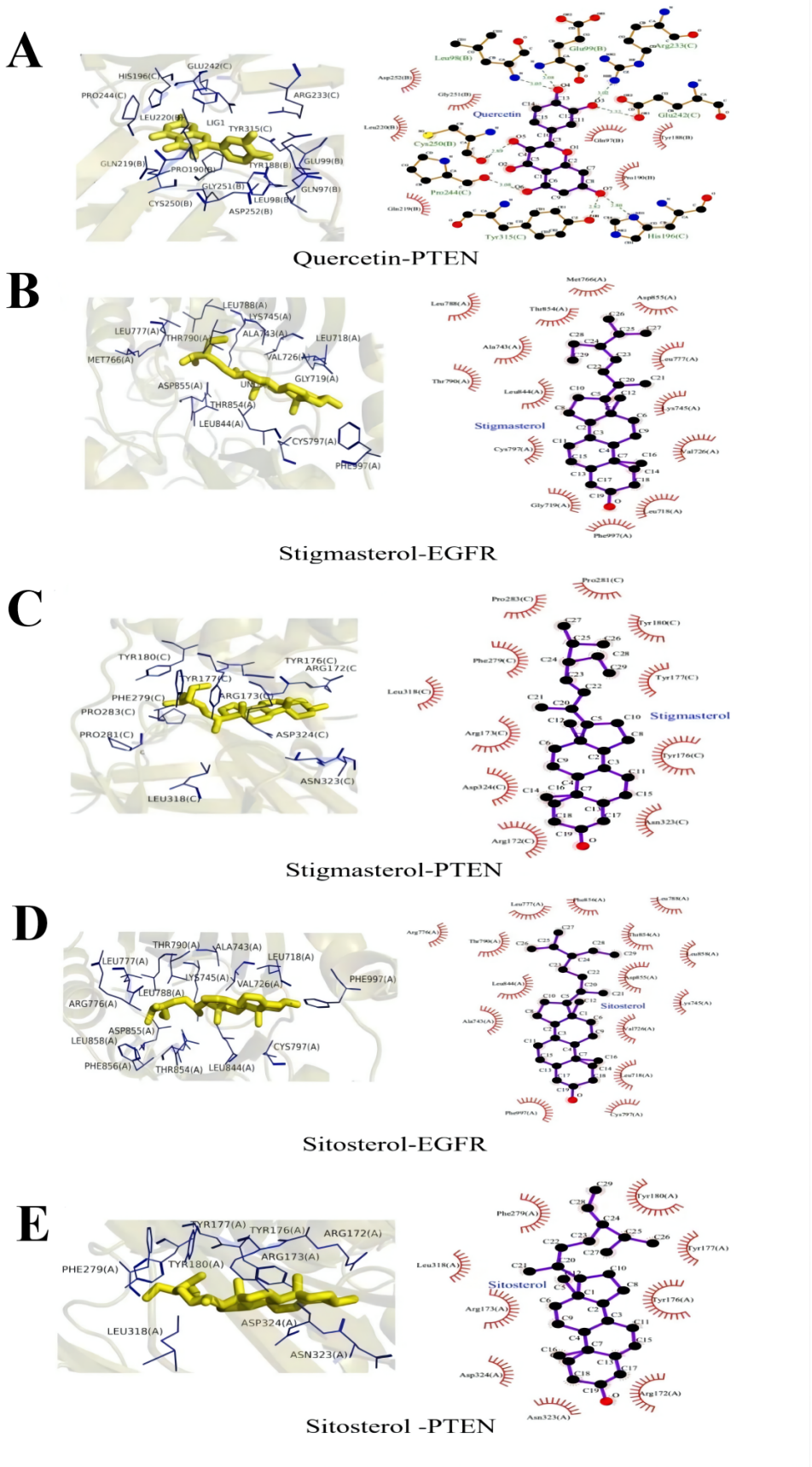

Fig. (11). 2D and 3D visualisation of docking results. *(A higher resolution / colour version of this figure is available in the electronic copy of the article).*

'SZY-YYH-SDH', was selected after data analysis. We then used the TCMSP and SwissTargetPrediction databases to predict and screen the main active ingredients of the three drugs and their targets and established the 'SZY-YYH-SDH' target dataset. The OMIM, GeneCards, and GEO databases were also used to search for targets related to PMO, and a disease target dataset was established. Their targets were intersected and imported into the STRING database to create PPI network diagrams and imported into Cytoscape 3.9.1 software for visualization. A total of 10 core targets were screened using the CytoHubba plug-in with the criteria of DC ≥ 2 times median, CC and BC ≥ median. The 24 intersecting targets were imported into the DAVID 6.8 database for GO, KEGG enrichment analysis, and finally, the pathway represented by the PI3K-Akt signalling pathway was obtained. They were also imported into the BioGps database for analysis of their distribution in human target organs. Finally, the targets enriched to the five core drug components (Quercetin, Luteolin, Stigmasterol, Sitosterol, Chryseriol) and PI3K-Akt signalling pathway were validated using AutoDockTools 1.5.6 and Autodocak vina, with the core PPI network in the molecular docking validation of six intersecting targets (VEGFA, TP53, AKT1, EGFR, MAPK1, PTEN) of the node showing that there was a tight binding relationship among EGFR, PTEN and Quercetin, Stigmasterol, Sitosterol, three components. The results of the molecular docking were visualised and analysed in 2D and 3D using Ligplot and Pymol software.

In this study, the active ingredients with the top 5 Degrees in the 'drugs-component-target-pathway-disease' network were screened. Quercetin is a flavonoid with a variety of pharmacological effects, including anti-inflammatory, antioxidant, and cardiovascular protection [12]. Yuan *et al*. found that Quercetin promoted BMSC proliferation and osteogenic differentiation and increased BMD and improved bone biomechanical properties in a devitalized rat model, possibly through inhibition of TNF-α, leading to nuclear factor-κB (NF-κB) activation and degradation of β-linked proteins by Quercetin [13]. Luteolin is also a flavonoid with a variety of pharmacological effects, including anti-inflammatory and anti-cancer [14, 15]. Kim *et al*. found that Luteolin reduced the differentiation of bone marrow monocytes and Raw264.7 cells into osteoclasts and inhibited osteoclast bone resorption [16]. Stigmasterol is a phytosterol with pharmacological properties that have a variety of pharmacological effects, such as anti-inflammatory, anti-atherosclerotic, and immunomodulatory [17-19]. Sitosterol is a major phytosterol found in plants and has been claimed for centuries to have many medical benefits, including anti-inflammatory, anti-allergic, and other pharmacological effects [20]. Wang *et al*. found that β-Sitosterol treatment of a rat model of glucocorticoid-induced osteoporosis attenuated the increase in bone resorption markers and the decrease in osteogenic markers, possibly due to β-Sitosterol's ability to mediate the regulation of the nuclear factor kappa-β ligand/osteoprotegerin and RunX2 pathways [21]. Chryseriol is a natural flavonoid with pharmacological effects, such as antioxidant, anti-inflammatory, and immunomodulatory [22]. Tai *et al*. found that Chryseriol significantly increased the growth of MC3T3-E1 cells and caused a significant elevation of alkaline phosphatase activity, collagen content, and nodule mineralization in the cells, confirming that Chryseriol may help prevent the development of osteoporosis [23].

The targets we enriched through the PI3K-Akt signalling pathway have a total of six intersecting targets with core nodes in the PPI network, namely VEGFA, TP53, AKT1, EGFR, MAPK1, and PTEN. Vascular endothelial growth factor A (VEGFA) is a heparin-binding pleiotropic cytokine produced by many cell types in the bone microenvironment, including endothelial cells and osteochondral lineage cells [24]. Yu *et al*. found that miR-16-5p was a target gene of VEGFA and showed a negative correlation with VEGFA [25]. Tumour protein p53 (TP53) is a transcription factor that is associated with cell cycle arrest, apoptosis, and metabolism and acts mainly as a suppressor of tumours [26-28]. Yu *et al*. [29] found that TP53 gene expression and serum p53 levels were upregulated in osteoporotic patients and mouse models of osteoporosis. It was also reported that hMSCs from patients with osteoporosis showed significantly higher expression of TP53 [25]. These findings suggest that p53 may play a central role in the development of osteoporosis. Akt is a family of three serine/threonine protein kinases (Akt1, Akt2, and Akt3) that regulate a host of cellular functions, including cell survival, proliferation, differentiation, and intermediary metabolism [30], and AKT1 is an overactive proto-oncogene in many cancers and is an important promoter of osteoblast-osteoclast coupling [31, 32]. Wang *et al*. demonstrated that Tanshinone modulates AKT1, promotes proliferation, and inhibits apoptosis in MSCs cells, and confirmed that Tanshinone ameliorates glucocorticoid-induced bone loss *via* activation of the AKT1 signalling pathway [33]. Epidermal growth factor receptor (EGFR) signalling is essential for tissue homeostasis and when activated, stimulates intracellular signalling cascades, such as Mitogen-activated protein kinases (MAPKs) and PI3Ks, which significantly affect cell behavior [34, 35]. Previous studies have found that EGFR-specific inhibitors or knockdown of EGFR in osteoblasts blocked EGFR activity in mice, leading to impaired bone formation [36]. In contrast, studies by Chandra and Yang *et al*. both found that osteoblast proliferation and apoptosis were regulated by the activation of EGFR, thereby promoting bone formation [37, 38]. MAPKs play an important role in cell proliferation, differentiation, and apoptosis as well as in the regulation of inflammation [39], while MAPK1 is a common gene in pathways, such as reactive oxygen species, PI3K-Akt signalling pathway, and TNF signalling pathway [40]. Xiao *et al*. found [41] that puerarin relies on the MAPK/NF-κB signalling pathway to inhibit osteoclastogenesis and thereby prevent bone resorption. The PTEN gene encodes a tumour suppressor protein that regulates the biological functions of many malignant tumours [42].

KEGG enrichment analysis of 24 intersecting targets of PMO 'SZY-YYH-SDH' further revealed that the drug molecules could exert regulatory effects through multiple pathways, including PI3K-Akt signalling pathway, focal adhesion, HIF-1 signalling pathway, thyroid hormone signalling pathway, and estrogen signalling pathway. Among them, the PI3K/Akt signalling pathway is an important mitogenic signalling pathway that plays an important role in a variety of cellular processes, including growth, survival, proliferation, and activity [43]. Akt has been reported to be closely associ-

ated with skeletal development, which is significantly delayed when the Akt1 gene is knocked out in rats, while downstream of Akt signalling can be regulated by regulating mTORC1/S6K1 protein to promote osteoblast differentiation and inhibit osteoblast apoptosis [44]. In addition, the PI3K/AKT pathway activates gene expression of osteogenic differentiation markers, such as OPN, ALP, and BMP-2, thereby promoting osteoblast differentiation and proliferation [45]. Conversely, it has been demonstrated that osteoclast differentiation and bone resorption capacity can be inhibited by inhibiting PI3K/AKT signaling [46]. Focal adhesions are specialized structures at the cellular-extracellular matrix contact points, where bundles of actin filaments are anchored to transmembrane receptors of the integrin family through a multimolecular complex of junctional plaque proteins, and are essential for bone development and osteocyte mechanotransduction [47, 48]. HIF-α pathway is the central regulator of the adaptive response to low oxygen levels and also plays a key role in angiogenesis-osteogenesis coupling [49]. Thyroid hormone signalling pathways have also been shown to play a key role in the regulation of bone growth, with thyroid hormone regulating other types of bone cells, such as chondrocytes, osteoblasts, osteoclasts, and insulin-like growth factor 1 [50, 51], while in most hyperthyroid states, low levels of thyroid stimulating hormone can directly affect bone [52]. It is well known that the decrease in estrogen levels after menopause is one of the main causes of osteoporosis in female patients [53]. Estrogen activates the Estrogen signalling pathway, and not only regulates bone resorption and promotes bone formation, but also regulates the differentiation of bone marrow mesenchymal stem cells into osteoblasts, maintaining the metabolic balance of bone cells [54, 55].

Molecular docking results showed that the binding energies between Quercetin-PTEN, Stigmasterol-EGFR, Stigmasterol- PTEN, Sitosterol - EGFR, and Sitosterol - PTEN were all ≤ -9.0 kcal·mol-1, indicating good binding between the components and targets activity. As shown in Fig. (**7**), Quercetin is derived from YYH, Stigmasterol from SZY and SDH, while Sitosterol belongs to the same three drugs. Therefore, we can speculate that the 'SZY-YYH-SDH' can act on PTEN and EGFR through Quercetin from YYH, Stigmasterol from SZY and SDH, Sitosterol from YYH, SZY, and SDH, and on PMO through the PI3K-Akt signalling pathway.

CONCLUSION

In this study, the active ingredients and potential targets of 'SZY-YYH-SDH' for the treatment of PMO were searched and analyzed. A total of 24 core nodes were identified, a PPI interaction network map was established, and the functions of the targets were correlated. In addition, this study screened five important components for the treatment of PMO, namely Quercetin, Luteolin, Stigmasterol, Sitosterol, and Chryseriol, and verified their binding activities with the core targets EGFR and PTEN using molecular docking techniques. In conclusion, this analysis by data mining, network pharmacology, and molecular docking techniques can provide some basis and reference for subsequent clinical studies on the treatment of PMO.

LIST OF ABBREVIATIONS

BP = Biological Process

CC = Cellular Component

DC = Degree Centrality

DEGs = Differential Genes

DL = Drug Similarity

MF = Molecular Function

OB = Oral Bioavailability

PMO = Postmenopausal Osteoporosis

PPI = Protein-protein Interaction

BC = Betweenness Centrality

ETHICS APPROVAL AND CONSENT TO PARTICIPATE

Not applicable.

HUMAN AND ANIMAL RIGHTS

No animals/humans were used in the studies that are the basis of this research.

CONSENT FOR PUBLICATION

Not applicable.

AVAILABILITY OF DATA AND MATERIALS

The data that support the findings of this study are available from the corresponding author upon reasonable request.

FUNDING

The authors would like to thank the financial support from the Science and Technology Development Program of Jilin Provincial Science and Technology Department, No: 20210101200JC. The funding source had a role in the design, execution, and decision to submit the manuscript for publication.

CONFLICT OF INTEREST

The authors declare no conflict of interest, financial or otherwise.

ACKNOWLEDGEMENTS

Declared none.

REFERENCES

[1] Yang, K.; Cao, F.; Xue, Y.; Tao, L.; Zhu, Y. Three classes of antioxidant defense systems and the development of postmenopausal osteoporosis. *Front. Physiol.,* **2022**, *13*, 840293. http://dx.doi.org/10.3389/fphys.2022.840293 PMID: 35309045

[2] Yu, B.; Wang, C.Y. Osteoporosis and periodontal diseases – An update on their association and mechanistic links. *Periodontol. 2000,* **2022**, *89*(1), 99-113. http://dx.doi.org/10.1111/prd.12422 PMID: 35244945

[3] Hsu, E.; Pacifici, R. From osteoimmunology to osteomicrobiology: How the microbiota and the immune system regulate bone. *Calcif. Tissue Int.,* **2018**, *102*(5), 512-521. http://dx.doi.org/10.1007/s00223-017-0321-0 PMID: 29018933

[4] Liu, P.; Wang, W.; Li, Z.; Li, Y.; Yu, X.; Tu, J.; Zhang, Z. Ferroptosis: A new regulatory mechanism in osteoporosis. *Oxid. Med. Cell. Longev.,* **2022**, *2022*, 1-10. http://dx.doi.org/10.1155/2022/2634431 PMID: 35082963

[5] Hamad, M.; Bajbouj, K.; Taneera, J. The case for an estrogen-iron axis in health and disease. Experimental and clinical endocrinology & diabetes: Official journal, german society of endocrinology. *Exp. Clin. Endocrinol. Diabetes,* **2020**, *128*(4), 270-277. http://dx.doi.org/10.1055/a-0885-1677 PMID: 30978727

[6] Kanis, J. A.; Cooper, C.; Rizzoli, R.; Reginster, J. Y. European guidance for the diagnosis and management of osteoporosis in postmenopausal women. *Osteoporosis Int.,* **2019**, *30*(1), 3-44. http://dx.doi.org/10.1007/s00198-018-4704-5

[7] Wu, W.T.; Li, Y.J.; Feng, A.Z.; Li, L.; Huang, T.; Xu, A.D.; Lyu, J. Data mining in clinical big data: The frequently used databases, steps, and methodological models. *Mil. Med. Res.,* **2021**, *8*(1), 44. http://dx.doi.org/10.1186/s40779-021-00338-z PMID: 34380547

[8] Yang, J.; Li, Y.; Liu, Q.; Li, L.; Feng, A.; Wang, T.; Zheng, S.; Xu, A.; Lyu, J. Brief introduction of medical database and data mining technology in big data era. *J. Evid. Based Med.,* **2020**, *13*(1), 57-69. http://dx.doi.org/10.1111/jebm.12373 PMID: 32086994

[9] Luo, T.; Lu, Y.; Yan, S.; Xiao, X.; Rong, X.; Guo, J. Network pharmacology in research of chinese medicine formula: Methodology, application and prospective. *Chin. J. Integr. Med.,* **2020**, *26*(1), 72-80. http://dx.doi.org/10.1007/s11655-019-3064-0 PMID: 30941682

[10] Kaur, T.; Madgulkar, A.; Bhalekar, M.; Asgaonkar, K. Molecular docking in formulation and development. *Curr. Drug Discov. Technol.,* **2019**, *16*(1), 30-39. http://dx.doi.org/10.2174/1570163815666180219112421 PMID: 29468973

[11] Tang, S.H.; Shen, D.; Yang, H.J. Analysis on composition rules of chinese patent drugs treating pain-related diseases based on data mining method. *Chin. J Integr. Med.,* **2019**, *25*(11), 861-866. http://dx.doi.org/10.1007/s11655-017-2957-z

[12] Chen, R.B.; Yang, Y.D.; Sun, K.; Liu, S.; Guo, W.; Zhang, J.X.; Li, Y. Potential mechanism of Ziyin Tongluo Formula in the treatment of postmenopausal osteoporosis: Based on network pharmacology and ovariectomized rat model. *Chin. Med.,* **2021**, *16*(1), 88. http://dx.doi.org/10.1186/s13020-021-00503-5 PMID: 34530875

[13] Yuan, Z.; Min, J.; Zhao, Y.; Cheng, Q.; Wang, K.; Lin, S.; Luo, J.; Liu, H. Quercetin rescued TNF-alpha-induced impairments in bone marrow-derived mesenchymal stem cell osteogenesis and improved osteoporosis in rats. *Am. J. Transl. Res.,* **2018**, *10*(12), 4313-4321. PMID: 30662673

[14] Aziz, N.; Kim, M.Y.; Cho, J.Y. Anti-inflammatory effects of luteolin: A review of *in vitro*, *in vivo* and *in silico* studies. *J. Ethnopharmacol.,* **2018**, *225*, 342-358. http://dx.doi.org/10.1016/j.jep.2018.05.019 PMID: 29801717

[15] Imran, M.; Rauf, A.; Abu-Izneid, T.; Nadeem, M.; Shariati, M.A.; Khan, I.A.; Imran, A.; Orhan, I.E.; Rizwan, M.; Atif, M.; Gondal, T.A.; Mubarak, M.S. Luteolin, a flavonoid, as an anticancer agent: A review. *Biomed Pharmacother.,* **2019**, *112*, 108612. http://dx.doi.org/10.1016/j.biopha.2019.108612

[16] Kim, T.H.; Jung, J.W.; Ha, B.G.; Hong, J.M.; Park, E.K.; Kim, H.J.; Kim, S.Y. The effects of luteolin on osteoclast differentiation, function *in vitro* and ovariectomy-induced bone loss. *J. Nutr. Biochem.,* **2011**, *22*(1), 8-15. http://dx.doi.org/10.1016/j.jnutbio.2009.11.002 PMID: 20233653

[17] Morgan, L.V.; Petry, F.; Scatolin, M.; de Oliveira, P.V.; Alves, B.O.; Zilli, G.A.L.; Volfe, C.R.B.; Oltramari, A.R.; de Oliveira, D.; Scapinello, J.; Müller, L.G. Investigation of the anti-inflammatory effects of stigmasterol in mice: Insight into its mechanism of action. *Behav. Pharmacol.,* **2021**, *32*(8), 640-651. http://dx.doi.org/10.1097/FBP.0000000000000658 PMID: 34657071

[18] Sampath, S.J.P.; Rath, S.N.; Kotikalapudi, N.; Venkatesan, V. Beneficial effects of secretome derived from mesenchymal stem cells with stigmasterol to negate IL-1β-induced inflammation *in-vitro* using rat chondrocytes-OA management. *Inflammopharmacology,* **2021**, *29*(6), 1701-1717. http://dx.doi.org/10.1007/s10787-021-00874-z PMID: 34546477

[19] Sharma, N.; Tan, M.A.; An, S.S.A. Phytosterols: Potential metabolic modulators in neurodegenerative diseases. *Int. J. Mol. Sci.,* **2021**, *22*(22), 12255. http://dx.doi.org/10.3390/ijms222212255 PMID: 34830148

[20] Marahatha, R.; Gyawali, K.; Sharma, K.; Gyawali, N.; Tandan, P.; Adhikari, A.; Timilsina, G.; Bhattarai, S.; Lamichhane, G.; Acharya, A.; Pathak, I.; Devkota, H.P.; Parajuli, N. Pharmacologic activities of phytosteroids in inflammatory diseases: Mechanism of action and therapeutic potentials. *Phytother. Res.,* **2021**, *35*(9), 5103-5124. http://dx.doi.org/10.1002/ptr.7138 PMID: 33957012

[21] Wang, T.; Li, S.; Yi, C.; Wang, X.; Han, X. Protective role of β-Sitosterol in glucocorticoid-induced osteoporosis in rats *via* the RANKL/OPG pathway. *Altern. Ther. Health Med.,* **2022**, *28*(7), 18-25. PMID: 35648689

[22] Yoon, H.S.; Park, C. Chrysoeriol ameliorates COX-2 expression through NF-κB, AP-1 and MAPK regulation *via* the TLR4/MyD88 signaling pathway in LPS-stimulated murine macrophages. *Exp. Ther. Med.,* **2021**, *22*(1), 718. http://dx.doi.org/10.3892/etm.2021.10150 PMID: 34007327

[23] Tai, B.H.; Cuong, N.M.; Huong, T.T.; Choi, E.M.; Kim, J.A.; Kim, Y.H. Chrysoeriol isolated from the leaves of *Eurya ciliata* stimulates proliferation and differentiation of osteoblastic MC3T3-E1 cells. *J. Asian Nat. Prod. Res.,* **2009**, *11*(9), 817-823. http://dx.doi.org/10.1080/10286020903117317 PMID: 20183330

[24] Buettmann, E. G.; McKenzie, J.A.; Migotsky, N.; Sykes, D.A.; Hu, P.; Yoneda, S.; Silva, M.J. VEGFA from early osteoblast lineage cells (Osterix^{+}) is required in mice for fracture healing. *J Bone Miner Res.,* **2019**, *34*(9), 1690-1706. http://dx.doi.org/10.1002/jbmr.3755

[25] Yu, T.; You, X.; Zhou, H.; He, W.; Li, Z.; Li, B.; Xia, J.; Zhu, H.; Zhao, Y.; Yu, G.; Xiong, Y.; Yang, Y. MiR-16-5p regulates postmenopausal osteoporosis by directly targeting VEGFA. *Aging,* **2020**, *12*(10), 9500-9514. http://dx.doi.org/10.18632/aging.103223 PMID: 32427128

[26] Rajandran, S.N.; Ma, C.A.; Tan, J.R.; Liu, J.; Wong, S.B.S.; Leung, Y.Y. Exploring the association of innate immunity biomarkers with MRI features in both early and late stages osteoarthritis. *Front. Med.,* **2020**, *7*, 554669. http://dx.doi.org/10.3389/fmed.2020.554669 PMID: 33282885

[27] Sun, G.; Ba, C.L.; Gao, R.; Liu, W.; Ji, Q. Association of IL-6, IL-8, MMP-13 gene polymorphisms with knee osteoarthritis susceptibility in the Chinese Han population. *Biosci. Rep.,* **2019**, *39*(2), BSR20181346. http://dx.doi.org/10.1042/BSR20181346 PMID: 30635366

[28] Christiansen, B.A.; Bhatti, S.; Goudarzi, R.; Emami, S. Management of osteoarthritis with avocado/soybean unsaponifiables. *Cartilage,* **2015**, *6*(1), 30-44. http://dx.doi.org/10.1177/1947603514554992 PMID: 25621100

[29] Yu, T.; You, X.; Zhou, H.; Kang, A.; He, W.; Li, Z.; Li, B.; Xia, J.; Zhu, H.; Zhao, Y.; Yu, G.; Xiong, Y.; Yang, Y. p53 plays a central role in the development of osteoporosis. *Aging,* **2020**, *12*(11), 10473-10487. http://dx.doi.org/10.18632/aging.103271 PMID: 32484789

[30] Arranz, A.; Doxaki, C.; Vergadi, E.; Martinez de la Torre, Y.; Vaporidi, K.; Lagoudaki, E.D.; Ieronymaki, E.; Androulidaki, A.; Venihaki, M.; Margioris, A.N.; Stathopoulos, E.N.; Tsichlis, P.N.; Tsatsanis, C. Akt1 and Akt2 protein kinases differentially contribute to macrophage polarization. *Proc. Natl. Acad. Sci. USA,* **2012**, *109*(24), 9517-9522. http://dx.doi.org/10.1073/pnas.1119038109 PMID: 22647600

[31] Wang, Z.; Qi, G.; Li, Z.; Cui, X.; Guo, S.; Zhang, Y.; Cai, P.; Wang, X. Effects of urolithin A on osteoclast differentiation induced by receptor activator of nuclear factor-κB ligand *via* bone morphogenic protein 2. *Bioengineered,* **2022**, *13*(3), 5064-5078. http://dx.doi.org/10.1080/21655979.2022.2036893 PMID: 35164658

[32] Mukherjee, A.; Rotwein, P. Selective signaling by Akt1 controls osteoblast differentiation and osteoblast-mediated osteoclast development. *Mol. Cell. Biol.,* **2012**, *32*(2), 490-500. http://dx.doi.org/10.1128/MCB.06361-11 PMID: 22064480

[33] Wang, Y.; Liu, L.; Qu, Z.; Wang, D.; Huang, W.; Kong, L.; Yan, L. Tanshinone ameliorates glucocorticoid-induced bone loss *via* activation of AKT1 signaling pathway. *Front. Cell Dev. Biol.,* **2022**, *10*, 878433. http://dx.doi.org/10.3389/fcell.2022.878433 PMID: 35419360

[34] Jia, H.; Ma, X.; Tong, W.; Doyran, B.; Sun, Z.; Wang, L.; Zhang, X.; Zhou, Y.; Badar, F.; Chandra, A.; Lu, X.L.; Xia, Y.; Han, L.; Enomoto-Iwamoto, M.; Qin, L. EGFR signaling is critical for maintaining the superficial layer of articular cartilage and preventing osteoarthritis initiation. *Proc. Natl. Acad. Sci.,* **2016**, *113*(50), 14360-14365. http://dx.doi.org/10.1073/pnas.1608938113 PMID: 27911782

[35] Filardo, E.J.; Quinn, J.A.; Bland, K.I.; Frackelton, A.R., Jr Estrogen-induced activation of Erk-1 and Erk-2 requires the G protein-coupled receptor homolog, GPR30, and occurs *via* trans-activation of the epidermal growth factor receptor through release of HB-EGF. *Mol. Endocrinol.,* **2000**, *14*(10), 1649-1660. http://dx.doi.org/10.1210/mend.14.10.0532 PMID: 11043579

[36] Zhang, X.; Tamasi, J.; Lu, X.; Zhu, J.; Chen, H.; Tian, X.; Lee, T.C.; Threadgill, D.W.; Kream, B.E.; Kang, Y.; Partridge, N.C.; Qin, L. Epidermal growth factor receptor plays an anabolic role in bone metabolism *in vivo*. *J Bone Miner Res.,* **2011**, *26*(5), 1022-34. http://dx.doi.org/10.1002/jbmr.295

[37] Chandra, A.; Lan, S.; Zhu, J.; Siclari, V.A.; Qin, L. Epidermal growth factor receptor (EGFR) signaling promotes proliferation and survival in osteoprogenitors by increasing early growth response 2 (EGR2) expression. *J. Biol. Chem.,* **2013**, *288*(28), 20488-20498. http://dx.doi.org/10.1074/jbc.M112.447250 PMID: 23720781

[38] Yang, F.; Lin, Z.W.; Huang, T.Y.; Chen, T.T.; Cui, J.; Li, M.Y.; Hua, Y.Q. Ligustilide, a major bioactive component of Angelica sinensis, promotes bone formation *via* the GPR30/EGFR pathway. *Sci. Rep.,* **2019**, *9*(1), 6991. http://dx.doi.org/10.1038/s41598-019-43518-7 PMID: 31061445

[39] Vanden Berghe, W.; Plaisance, S.; Boone, E.; De Bosscher, K.; Schmitz, M.L.; Fiers, W.; Haegeman, G. p38 and extracellular signal-regulated kinase mitogen-activated protein kinase pathways are required for nuclear factor-kappaB p65 transactivation mediated by tumor necrosis factor. *J. Biol. Chem.,* **1998**, *273*(6), 3285-3290. http://dx.doi.org/10.1074/jbc.273.6.3285 PMID: 9452444

[40] Shuai, Y.; Jiang, Z.; Yuan, Q.; Tu, S.; Zeng, F. Deciphering the underlying mechanism of eucommiae cortex against osteoporotic fracture by network pharmacology. *Evid. Based Complement Alternat. Med.,* **2020**, *2020*, 7049812. http://dx.doi.org/10.1155/2020/7049812

[41] Xiao, L.; Zhong, M.; Huang, Y.; Zhu, J.; Tang, W.; Li, D.; Shi, J.; Lu, A.; Yang, H.; Geng, D.; Li, H.; Wang, Z. Puerarin alleviates osteoporosis in the ovariectomy-induced mice by suppressing osteoclastogenesis *via* inhibition of TRAF6/ROS-dependent MAPK/NF-κB signaling pathways. *Aging,* **2020**, *12*(21), 21706-21729. http://dx.doi.org/10.18632/aging.103976 PMID: 33176281

[42] Ghafouri-Fard, S.; Abak, A.; Shoorei, H.; Mohaqiq, M.; Majidpoor, J.; Sayad, A.; Taheri, M. Regulatory role of microRNAs on PTEN signaling. *Biomed Pharmacother.,* **2021**, *133*, 110986. http://dx.doi.org/10.1016/j.biopha.2020.110986

[43] Alzahrani, A.S. PI3K/Akt/mTOR inhibitors in cancer: At the bench and bedside. *Semin. Cancer Biol.,* **2019**, *59*, 125-132. http://dx.doi.org/10.1016/j.semcancer.2019.07.009 PMID: 31323288

[44] Guo, K.; Wang, T.; Luo, E.; Leng, X.; Yao, B. Use of network pharmacology and molecular docking technology to analyze the mechanism of action of velvet antler in the treatment of postmenopausal osteoporosis. *Evid Based Complement Alternat Med.,* **2021**, *2012*, 7144529. http://dx.doi.org/10.1155/2021/7144529

[45] Wu, C.M.; Chen, P.C.; Li, T.M.; Fong, Y.C.; Tang, C.H. Si-Wu-tang extract stimulates bone formation through PI3K/Akt/NF-κB signaling pathways in osteoblasts. *BMC Complement. Altern. Med.,* **2013**, *13*(1), 277. http://dx.doi.org/10.1186/1472-6882-13-277 PMID: 24156308

[46] Gong, W.; Chen, X.; Shi, T.; Shao, X.; An, X.; Qin, J.; Chen, X.; Jiang, Q.; Guo, B. Network pharmacology-based strategy for the investigation of the anti-osteoporosis effects and underlying mechanism of zhuangguguanjie formulation. *Front. Pharmacol.,* **2021**, *12*, 727808. http://dx.doi.org/10.3389/fphar.2021.727808 PMID: 34658868

[47] Qin, L.; Liu, W.; Cao, H.; Xiao, G. Molecular mechanosensors in osteocytes. *Bone Res.,* **2020**, *8*(1), 23. http://dx.doi.org/10.1038/s41413-020-0099-y PMID: 32550039

[48] Zintzaras, E.; Doxani, C.; Koufakis, T.; Kastanis, A.; Rodopoulou, P.; Karachalios, T. Synopsis and meta-analysis of genetic association studies in osteoporosis for the focal adhesion family genes: The CUMAGAS-OSTEOporosis information system. *BMC Med.,* **2011**, *9*(1), 9. http://dx.doi.org/10.1186/1741-7015-9-9 PMID: 21269451

[49] Yang, M.; Li, C.J.; Sun, X.; Guo, Q.; Xiao, Y.; Su, T.; Tu, M.L.; Peng, H.; Lu, Q.; Liu, Q.; He, H.B.; Jiang, T.J.; Lei, M.X.; Wan, M.; Cao, X.; Luo, X.H. MiR-497~195 cluster regulates angiogenesis during coupling with osteogenesis by maintaining endothelial Notch and HIF-1α activity. *Nat. Commun.,* **2017**, *8*(1), 16003. http://dx.doi.org/10.1038/ncomms16003 PMID: 28685750

[50] Duncan Bassett, J.H.; Williams, G.R. The molecular actions of thyroid hormone in bone. *Trends Endocrinol. Metab.,* **2003**, *14*(8), 356-364. http://dx.doi.org/10.1016/S1043-2760(03)00144-9 PMID: 14516933

[51] Kim, H.Y.; Mohan, S. Role and mechanisms of actions of thyroid hormone on the skeletal development. *Bone Res.,* **2013**, *1*(2), 146-161. http://dx.doi.org/10.4248/BR201302004 PMID: 26273499

[52] Baliram, R.; Sun, L.; Cao, J.; Li, J.; Latif, R.; Huber, A.K.; Yuen, T.; Blair, H.C.; Zaidi, M.; Davies, T.F. Hyperthyroid-associated osteoporosis is exacerbated by the loss of TSH signaling. *J. Clin. Invest.,* **2012**, *122*(10), 3737-3741. http://dx.doi.org/10.1172/JCI63948 PMID: 22996689

[53] Wu, D.; Cline-Smith, A.; Shashkova, E.; Perla, A.; Katyal, A.; Aurora, R. T-cell mediated inflammation in postmenopausal osteoporosis. *Front. Immunol.,* **2021**, *12*, 687551. http://dx.doi.org/10.3389/fimmu.2021.687551 PMID: 34276675

[54] Faltas, C.L.; LeBron, K.A.; Holz, M.K. Unconventional estrogen signaling in health and disease. *Endocrinology,* **2020**, *161*(4), bqaa030. http://dx.doi.org/10.1210/endocr/bqaa030 PMID: 32128594

[55] Fischer, V.; Haffner-Luntzer, M. Interaction between bone and immune cells: Implications for postmenopausal osteoporosis. *Semin. Cell Dev. Biol.,* **2022**, *123*, 14-21. http://dx.doi.org/10.1016/j.semcdb.2021.05.014 PMID: 34024716